Terahertz-Driven Local Dipolar Correlation in a Quantum Paraelectric

Bing Cheng,[1,*] Patrick L. Kramer,[2] Zhi-Xun Shen,[1,3,4] and Matthias C. Hoffmann[2,†]

[1]*Stanford Institute for Materials and Energy Sciences, SLAC National Accelerator Laboratory, Menlo Park, California 94025, USA*
[2]*Laser Science and Technology, SLAC Linear Accelerator Laboratory, Menlo Park, California 94025, USA*
[3]*Geballe Laboratory for Advanced Materials, Stanford University, Stanford, California 94305, USA*
[4]*Departments of Physics and Applied Physics, Stanford University, Stanford, California 94305, USA*

Light-induced ferroelectricity in quantum paraelectrics is a new avenue of achieving dynamic stabilization of hidden orders in quantum materials. In this Letter, we explore the possibility of driving a transient ferroelectric phase in the quantum paraelectric $KTaO_3$ via intense terahertz excitation of the soft mode. We observe a long-lived relaxation in the terahertz-driven second harmonic generation (SHG) signal that lasts up to 20 ps at 10 K, which may be attributed to light-induced ferroelectricity. Through analyzing the terahertz-induced coherent soft-mode oscillation and finding its hardening with fluence well described by a single-well potential, we demonstrate that intense terahertz pulses up to 500 kV/cm cannot drive a global ferroelectric phase in $KTaO_3$. Instead, we find the unusual long-lived relaxation of the SHG signal comes from a terahertz-driven moderate dipolar correlation between the defect-induced local polar structures. We discuss the impact of our findings on current investigations of the terahertz-induced ferroelectric phase in quantum paraelectrics.

In quantum paraelectrics (QPEs), e.g., $SrTiO_3$, complete softening of their soft polar modes is prevented by the nuclear zero-point vibration [1]. Such quantum fluctuation hinders QPEs to develop long-range ferroelectric orders down to millikelvins even if a shallow ferroelectric (FE) double-well potential indeed forms below the FE Curie temperatures [1,2]. In recent decades, there has been strong interest in recovering the hidden FE phase in QPEs by means of doping and straining [3–5]. Until recently, rapid advances in ultrafast laser technology have opened the possibility of driving QPEs into a transient FE phase by intense laser pulses [6]. However, the experimental evidence is ambiguous and the precise mechanism remains debated. According to a quantum-mechanical model developed for photoexcited phases in $SrTiO_3$, the resonant terahertz excitation of the FE soft mode could tune the lattice strain in a nonmechanical fashion, which transiently produces a deep double-well potential along the soft-mode coordinate and drives a mixture of the lattice wave functions of the ground and first excited states. The mixture creates a nonzero expectation value of the soft-mode displacement and triggers a transient ferroelectricity [7]. This transient FE phase breaks global lattice inversion symmetry and contributes an ultrafast and long-lived second harmonic generation (SHG) relaxation to the time-resolved SHG measurement, which has been claimed to be observed in $SrTiO_3$ by recent experimental works [8,9].

Despite the exciting progress of the terahertz-induced transient FE phase in QPEs, some experimental challenges still exist. First, although the long-lived SHG relaxation has been observed experimentally and interpreted as the fingerprint of a transient FE phase [8], the temporal dynamics of the FE soft mode, a more intrinsic landmark of the transient FE phase, is still uncharted. In a double-well lattice potential (ferroelectric phase), the ladder of vibrational energy eigenstates shows decreasing energy spacings as the eigenstate's index increases [10]. Intense terahertz excitation of the soft mode will populate excited lattice states and yield a redshift of the soft-mode frequency. On the other hand, a terahertz-driven FE phase is predicted to accompany a light-induced deepening of the double-well potential [7], transiently increasing the energy spacings between the vibrational eigenstates. Therefore, as driven into a transient FE phase, it is not yet clear whether the FE soft mode in QPEs will soften, harden, or exhibit more complicated temporal behaviors. Second, defects and impurities usually cannot be avoided in crystals. In perovskite-type QPEs, which are highly polarizable hosts, unavoidable defects and impurities always carry dipolar entities that can polarize nearby regions and develop to polar nanoregions (PNRs) [11]. At the temperatures far above FE Curie temperature, these PNRs are small and behave like noninteracting pointlike dipoles [11]. As temperature decreases, the size and amount of PNRs grow. Even if a global FE order does not develop in QPEs, these randomly oriented PNRs can be aligned by terahertz pulses and contribute signals to terahertz-pumped SHG probe measurements, complicating the observation of an intrinsic light-induced FE phase.
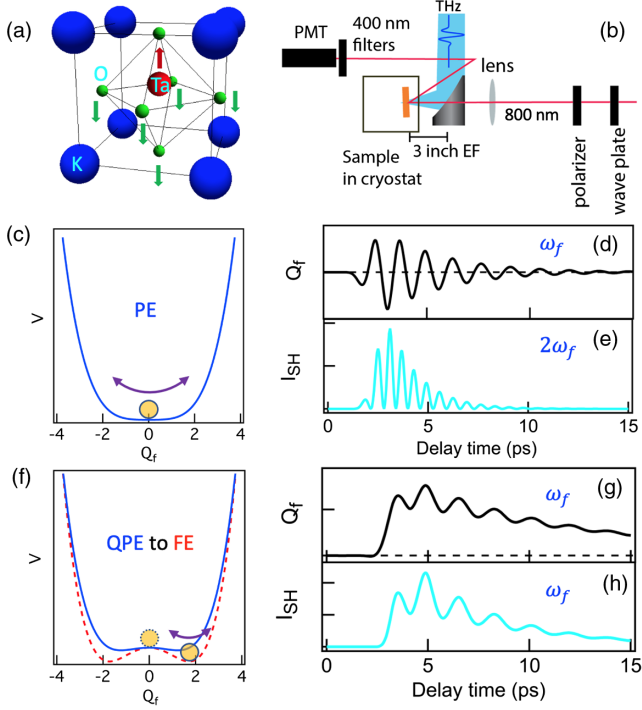
FIG. 1. (a) The cubic lattice structure and ferroelectric soft mode of $KTaO_3$. (b) Schematic illustration of our terahertz pump SHG probe setup. PMT: photomultiplier tube, EF: effective focal length. (c) Illustration of the single-well lattice potential along the soft-mode coordinate Q_f in paraelectric (PE) state. (d),(e) Illustration of terahertz-driven soft-mode displacement Q_f and terahertz-induced SHG intensity I_{SH} as a function of delay time in the lattice potential shown in (c). Note that $I_{SH} \propto Q_f^2(t)$. Hence, the oscillating frequency of I_{SH} is the double of the fundamental soft-mode frequency. (f) Illustration of the ultrafast deepening of the FE potential along the soft-mode coordinate Q_f in a terahertz-driven transient FE phase. Note that the soft mode will be driven to oscillate in a new potential minimum. (g), (h) Illustration of possible soft-mode displacement Q_f and terahertz-induced SHG signal as a function of delay time in a terahertz-driven transient FE phase. Because of being driven to a new potential minimum, Q_f will include a nonoscillatory component. The oscillation of I_{SH} follows the oscillation of Q_f and will not show a simple frequency doubling.

In this Letter, we used terahertz pump SHG probe spectroscopy to study the quantum paraelectric $KTaO_3$ and revisited the problem of the terahertz-induced FE phase in QPEs. $KTaO_3$ is a counterpart of $SrTiO_3$, but has a very low FE Curie temperature $T_c \sim 4$ K extrapolated from the Curie-Weiss fit to the high-temperature permittivity [12]. Unlike $SrTiO_3$, $KTaO_3$ does not experience any structural phase transitions below room temperature down to millikelvins [Fig. 1(a)] [13], avoiding the complicated phonon dynamics in $SrTiO_3$ [14–16]. Through analyzing the terahertz-induced SHG signal, we demonstrated that a terahertz field up to 500 kV/cm cannot drive a global transient FE phase in $KTaO_3$. Instead, we found the intense
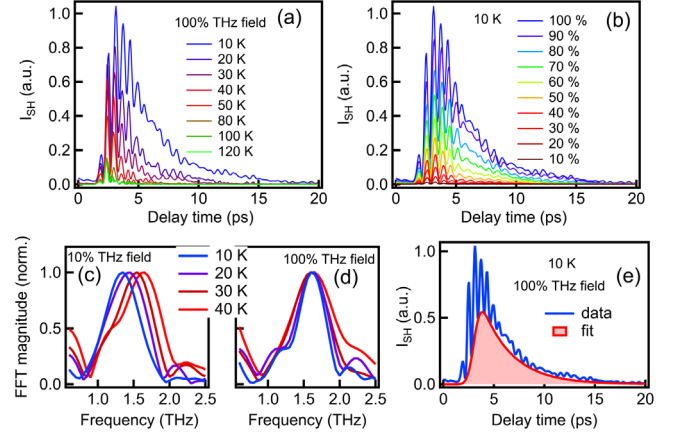

FIG. 2. (a) Temperature-dependent time-resolved SHG signals recorded at maximum terahertz field strength. (b) Terahertz field strength-dependent time-resolved SHG signals at 10 K. The terahertz field is attenuated in 10% steps. (c),(d) Temperature-dependent Fourier transform of time-resolved SHG signal pumped with 10% and 100% of maximum terahertz field strength respectively. (e) A single exponential relaxation fit to the non-oscillatory SHG relaxation.

terahertz field drives moderate dipolar correlation between local polar nanoregions, contributing remarkable long-lived SHG relaxation persisting up to 20 ps to the time-resolved SHG measurement.

The soft mode in $KTaO_3$ is an infrared-active phonon mode [Fig. 1(a)] and downshifts to ~0.8 THz below 50 K [17–19]. Thus, terahertz pulses can resonantly drive large coherent soft-mode oscillation, which transiently breaks global lattice inversion symmetry and introduces a time-dependent second order susceptibility $\chi^{(2)}$ [20]. We used single-cycle terahertz pulses up to 500 kV/cm generated from optical rectification in $LiNbO_3$ to excite a $KTaO_3$ single crystal. The resultant SHG at 400 nm was probed by a 130 fs, 800 nm pulse as a function of time delay with respect to the terahertz pump pulse. The schematic of our terahertz pump SHG probe setup is shown in Fig. 1(b). More details can be found in the Supplemental Material [21].

Figure 2(a) shows terahertz-induced SHG intensity as a function of delay time at various temperatures. At temperatures above 80 K, the transient SHG signal is weak and primarily follows the waveform of terahertz pulse *squared*. As temperature decreases, the SHG signal grows rapidly. In the meantime, a clear oscillatory feature develops on top of a nonoscillatory SHG background. At 10 K, the terahertz field drives large SHG oscillations, as well as a significant nonoscillatory SHG component that persists to 20 ps. Similar long-lived nonoscillatory SHG relaxation has been observed in $SrTiO_3$ and interpreted to the signature of a transient FE order [8]. We will discuss the origin of the long-lived SHG relaxation in $KTaO_3$ later. Figure 2(c) shows a fast Fourier transform analysis of SHG oscillations

at 10% of full terahertz field strength. At 40 K, a single mode at 1.6 THz emerges. As temperature decreases, this mode continuously softens, consistent with the well-known behavior of the KTaO$_3$ soft mode [17–19]. Figure 2(d) shows temperature-dependent Fourier transforms of SHG oscillations under a full terahertz excitation. The mode frequencies blueshift comparing to the data in Fig. 2(c). Note that, in our measurements, the frequency of the SHG signal is twice that of the fundamental soft-mode frequency [17–19]. This frequency doubling is expected in a centrosymmetric system with single-well potential. As shown in Fig. 1(c), if an oscillator is driven in a single-well lattice potential, in each cycle, the driven displacement $Q_f(t)$ will cross $Q_f = 0$ twice [Fig. 1(d)]. Because of the SHG intensity $I_{SH}(t) \propto |\chi^{(2)}t|^2 \propto Q_f^2(t)$ [20], the frequency of the SHG oscillation will be the double of the oscillating frequency of driven displacement $Q_f(t)$ [Fig. 1(e)].

In Fig. 2(b), we show a terahertz-induced SHG signal at 10 K under various terahertz field strengths (in 10% step). One can see the oscillatory and nonoscillatory components of the SHG signal both rise rapidly with increasing pump field strength. The SHG signal is tied to temporal evolution of symmetry changes and carries intrinsic information of the soft-mode lattice potential. To isolate the pure oscillatory component, we used a single exponential relaxation function $\exp(-t/\tau_0)$ convolving with the step function to capture the nonoscillatory SHG background. One simulation example was displayed in Fig. 2(e). Note that the oscillatory component of the SHG signal is proportional to $Q_f^2(t)$ and always positive. Hence, the simulating curve for the nonoscillatory background should capture the bottoms of the oscillation on the SHG signal. After subtracting the nonoscillatory component, we plot the pure oscillatory SHG components and their Fourier transforms at 10 K in Figs. 3(a) and 3(b), respectively. One remarkable feature one can quickly notice in both plots is the hardening of the soft mode as the terahertz field strength increases, which is a typical characteristic of a driven oscillator in an anharmonic lattice potential [22]. In a quartic anharmonic lattice potential $V(Q_f) = \frac{1}{2}M\omega_{f0}^2 Q_f^2 + \frac{1}{4}MkQ_f^4$ [Fig. 1(c)], the soft-mode frequency approximately follows $\omega_f^2 = \omega_{f0}^2 + 3kQ_f^2$ [22]. Here ω_{f0} is the soft-mode frequency in the harmonic limit, M is the soft-mode reduced mass, k is the coefficient of the quartic term, and Q_f is the field-driven soft-mode displacement. As Q_f increases, the soft mode will naturally harden. In our measurement, we cannot measure Q_f directly, but the terahertz-driven $Q_f^2(t)$ is proportional to the oscillatory SHG signal $I_{SH}(t)$. Therefore, $I_{SH}(t)$ and $Q_f^2(t)$ should have similar temporal waveforms in the time domain. We numerically solved the soft-mode motion equation,

$$\frac{d^2Q_f}{dt^2} + \gamma\frac{dQ_f}{dt} + \omega_{f0}^2 Q_f + kQ_f^3 = \frac{Z^* eE_{in}}{M}. \quad (1)$$
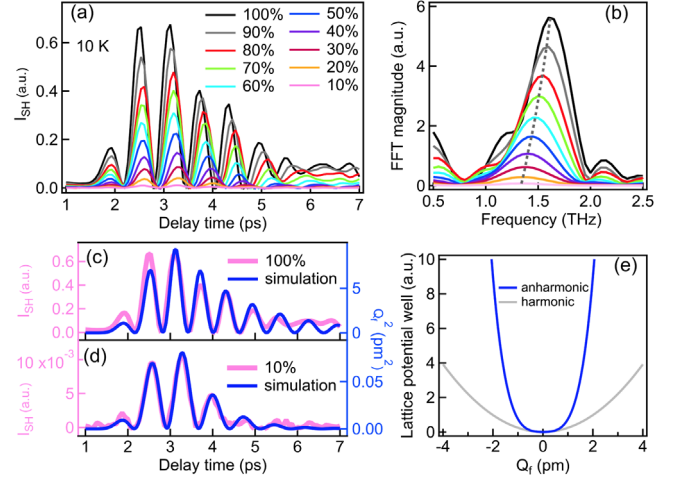

FIG. 3. (a) The pure oscillatory SHG signals recorded under various terahertz field strengths at 10 K. The maximum (100%) terahertz field strength is 500 kV/cm. (b) The Fourier transforms of oscillatory SHG signals in (a). The gray dashed curve indicates the hardening trend of the FE soft mode as increasing terahertz field strength. (c),(d) Numerical simulations of terahertz-driven soft-mode displacement squared Q_f^2 using Eq. (1) pumped by 100% and 10% of maximum terahertz field strength, respectively. Because of $I_{SH} \propto Q_f^2(t)$, $I_{SH}(t)$ (left axis) and $Q_f^2(t)$ (right axis) have similar temporal waveform. (e) The experimentally reconstructed anharmonic potential of the FE soft mode plotted along with the harmonic potential.

Here γ is the damping coefficient, $Z^* = 8.6$ is the soft-mode Born effective charge [23], e is the charge of electron, and E_{in} is the terahertz field inside KTaO$_3$. The reduced mass M is determined by $[1/(M_K + M_{Ta}) + 1/(3M_O)]^{-1}$, and M_K, M_{Ta}, and M_O are the atomic masses of potassium, tantalum, and oxygen, respectively [10]. More simulation details can be found in the Supplemental Material [21]. We plot oscillatory SHG data and the numerically simulated $Q_f^2(t)$ together in Figs. 3(c) and 3(d). One can see the simulations well reproduce the waveforms of the oscillatory SHG signal in the time domain. The harmonic soft-mode frequency $\omega_{f0}/2\pi$ and the quartic anharmonic coefficient k were found to be 0.7 and 2.0 pm^{-2} THz^2, respectively. The damping coefficient γ decreases as the terahertz field increases and was found to be $\sim 2\pi \times 0.11$ THz under a full terahertz excitation. The experimentally reconstructed soft-mode anharmonic potential was plotted in Fig. 3(e) along with the harmonic potential of the FE soft mode, similar to the single-well soft-mode lattice potential reconstructed in a 300-nm-thick SrTiO$_3$ film utilizing intense terahertz transmission spectroscopy [24].

Our analysis of the coherent soft-mode oscillation has provided critical insights on the origin of the observed long-lived and nonoscillatory SHG relaxation in KTaO$_3$. We showed that a single-well quartic lattice potential model [Eq. (1)] can well reproduce all 10 K SHG oscillations. Most importantly, the quartic coefficient k of the potential is found to be not sensitive to the terahertz field strength

(see the Supplemental Material [21]). The potential profile does not experience detectable changes as pump field strength increases to 500 kV/cm. Moreover, in such an anharmonic potential [Fig. 3(e)], the terahertz-driven soft-mode hardening is actually adverse to stabilize a FE phase. The large terahertz-driven magnitude of $Q_f^2(t)$, which acts like an enhanced thermal-averaged $\langle Q_f^2 \rangle$ by elevating temperature [22], should drive $KTaO_3$ into a deep para-electric phase. In this regard, the nonoscillatory component of the SHG signal, despite persisting to 20 ps at 10 K, is unlikely from a global light-induced FE phase transition.

To explore its origin, we employed detailed analysis of the nonoscillatory SHG component. We used a single exponential relaxation function to extract the pump-probe amplitude I_0 and relaxation time τ_0 [Fig. 2(d)]. More fitting details can be found in the Supplemental Material [21]. We plot I_0 and τ_0 as a function of temperature under maximum terahertz field excitation in Figs. 4(a) and 4(b). At temperatures above 80 K, I_0 is negligible and τ_0 is ~400 fs. As temperature decreases, both quantities surge. Their onset temperatures, ~60 K, coincide with the temperature reported for local polar structures arising in $KTaO_3$ [11,25].

It is well established that, even if in nominally pure perovskite-type QPEs, the unavoidable impurities and defects usually bring in dipolar entities that could develop to local polar structures at the nanometer scale [11]. In pure $KTaO_3$, the defects are mainly from the Ta^{+3}/Ta^{+4} and oxygen vacancies [26,27] which introduce PNRs below ~50 K [25,28]. These PNRs break local lattice inversion symmetry but orient randomly, which has been reported to contribute a weak and incoherent SHG background signal to static SHG measurement below 50–60 K [26,29]. In our measurement, the randomly oriented PNRs can be transiently polarized by terahertz electric field and contribute a large initial amplitude to the terahertz-induced SHG signal. As terahertz pulses are turned off, the polarized PNRs will gradually depolarize, resulting in a temporal SHG relaxation as a function of delay time.

Figures 4(c) and 4(d) show the terahertz-induced SHG amplitude I_0 and relaxation time τ_0 as functions of terahertz field strength. At 40 K, I_0 grows slowly and linearly with increasing terahertz field, and τ_0 is insensitive to terahertz field strength. The increase of the SHG amplitude seems to not modify the relaxation process. Such behavior implies the PNRs at 40 K act like noninteracting dipolar entities. In contrast, at 10 K, I_0 rises in a highly nonlinear fashion as a function of terahertz field strength, which is quite similar to the observation in $SrTiO_3$ [8]. The relaxation time τ_0 at lowest field strength is 1.5 ps, close to the values of 40 K. As terahertz field strength increases, τ_0 grows rapidly and then gradually saturates at 3 ps. The large increase of τ_0 strongly indicates a marked dipolar correlation between PNRs develops under high terahertz field excitation. It had been noted before that the polarized dipoles with close neighbors would take a longer time to depolarize than
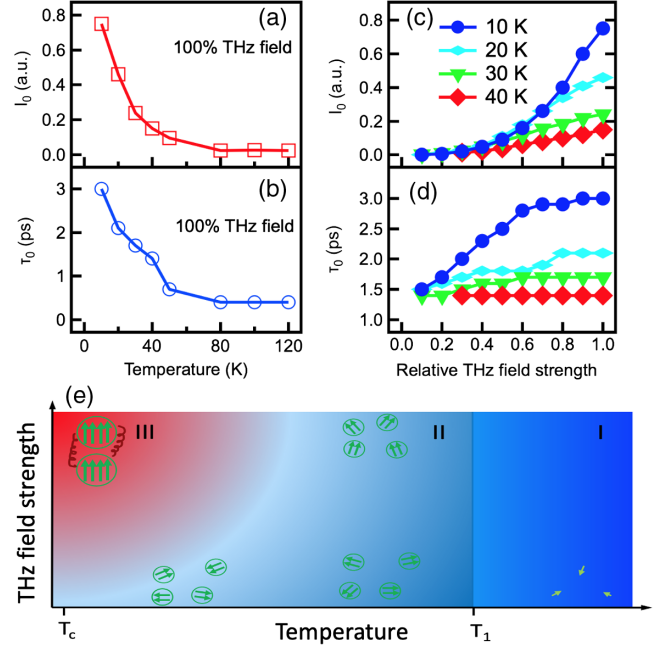

FIG. 4. (a),(b) The pump-probe magnitude I_0 and relaxation time τ_0 of terahertz-induced nonoscillatory SHG component as a function of temperature under maximum terahertz excitation. (c),(d) The pump-probe magnitude I_0 and relaxation time τ_0 of terahertz-induced nonoscillatory SHG component as a function of terahertz field strength at different temperatures. (e) A qualitative phase diagram of PNR dynamics in the terahertz-pumped $KTaO_3$. $T_1 \sim 60$ K is the onset temperature of PNRs. $T_c \sim 4$ K is the FE Curie temperature. Above T_1, as shown in region I, the pointlike dipoles are dominant. Below T_1, PNRs start to appear. In region II, these PNRs behave like noninteracting dipolar entities, even if they are partially polarized by strong terahertz pulses. As temperature is further lowered, as shown in region III, strong terahertz pulses not only polarize PNRs, they also enhance the dipolar interaction between PNRs and induce longer depolarization relaxation.

normal isolated dipoles once the polarizing field is turned off [30]. In our case, as more PNRs are polarized by the terahertz field at the lowest temperature, parts of PNR pairs will tend to be bound at a temporal potential minimum of the dipole-dipole interaction Hamiltonian, which eventually prevents them from depolarizing rapidly as usual and results in a longer relaxation [30]. Despite more efforts required to fully understand the process, it is clear that such terahertz-field-enhanced correlation is the primary reason for the long-lived SHG relaxation persisting up to 20 ps.

A qualitative phase diagram of PNR dynamics in the terahertz-pumped $KTaO_3$ is displayed in Fig. 4(e). In addition to the polarizing and depolarizing dynamics of PNRs, the most striking feature is the emergence of a terahertz-enhanced dipolar correlation region (region III) at low temperatures and high terahertz field strengths. This phase diagram is constructed from our results of $KTaO_3$, but it could be applied to other QPEs where the response of PNRs dominates.

Finally, we would like to make remarks on the general relevance of our findings to current investigations of the terahertz-induced FE phase in QPEs. Our work provides a standard protocol to disentangle the nonoscillatory and oscillatory components of a terahertz-induced SHG signal. We showed a light-induced FE phase is not the only possible origin of the observed long-lived nonoscillatory SHG relaxation in QPEs. The local polar structures formed at low temperatures, along with the terahertz-enhanced dipolar correlation between them, can also result in such a long-lived SHG relaxation persisting up to 20 ps. It is noteworthy that the amplitude of nonoscillatory SHG relaxation in $KTaO_3$ is an increasing function of terahertz field strength [Fig. 4(c)], which is distinct from the expected field evolution of the SHG relaxation in a terahertz-induced transient FE phase. In the transient FE phase predicted by a quantum model [7], the global FE polarization comes from the terahertz-driven mixture of the ground and first excited states of the lattice wave functions. As terahertz field strength reaches a threshold, more higher excited lattice states will be populated. Such an overpopulated and light-mixed lattice state behaves like a normal thermally excited paraelectric state that will suppress the global FE polarization [7]. The terahertz-induced order parameter (global FE polarization), or equivalently, the nonoscillatory SHG relaxation amplitude, should show a nonmonotonic field evolution (increases first and then decreases) [7]. Hence, our observation is crucial and imposes strong restrictions on interpreting the terahertz-induced long-lived SHG relaxation to the signature of a transient FE phase.

A more convincing way to demonstrate a terahertz-induced FE phase is to track the temporal dynamics of the FE soft mode. In a light-induced FE phase, the soft mode will be driven to oscillate at a new potential minimum ($Q_f \neq 0$) transiently [Fig. 1(f)]. The resultant coherent oscillation of soft-mode displacement [Fig. 1(g)] will not cross $Q_f = 0$ as long as the transient FE phase has not degenerated significantly [Fig. 1(f)]. Therefore, the oscillatory component of SHG, despite still being proportional to Q_f^2 [Fig. 1(h)], will closely follow the oscillation of the soft-mode displacement $Q_f(t)$ rather than only showing frequency doubling [Fig. 1(g)]. Careful analysis of the soft-mode trajectory in the time domain and the soft-mode hardening or softening in the frequency domain, as we demonstrated in $KTaO_3$, will enable one to extract information of or even reconstruct the light-induced double-well potential of the transient FE phase.

In summary, we used terahertz pump SHG probe spectroscopy to study the possibility of driving a quantum paraelectric $KTaO_3$ into a transient FE phase. We started by analyzing the soft-mode oscillations revealed by the SHG probe and found that the observed hardening of the soft mode can be described by a single-well potential, distinct from what is expected from a terahertz-induced FE phase.

We demonstrated the long-lived nonoscillatory SHG relaxation at 10 K, despite seemingly from a transient FE phase, actually results from the terahertz-induced moderate dipolar correlation between the defect-induced local polar structures. Our results are in agreement with current theoretical predictions and pave the road for the realization of a terahertz-induced FE phase in QPEs unambiguously.

———————————

[*]chengbing986@gmail.com
[†]hoffmann@slac.stanford.edu

[1] K. A. Müller and H. Burkard, Phys. Rev. B **19**, 3593 (1979).
[2] D. Shin, S. Latini, C. Schäfer, S. A. Sato, U. De Giovannini, H. Hübener, and A. Rubio, Phys. Rev. B **104**, L060103 (2021).
[3] J. G. Bednorz and K. A. Müller, Phys. Rev. Lett. **52**, 2289 (1984).
[4] M. Itoh, R. Wang, Y. Inaguma, T. Yamaguchi, Y.-J. Shan, and T. Nakamura, Phys. Rev. Lett. **82**, 3540 (1999).
[5] J. Haeni, P. Irvin, W. Chang, R. Uecker, P. Reiche, Y. L. Li, S. Choudhury, W. Tian, M. E. Hawley, B. Craigo et al., Nature (London) **430**, 758 (2004).
[6] A. Subedi, Phys. Rev. B **95**, 134113 (2017).
[7] D. Shin, S. Latini, C. Schäfer, S. A. Sato, E. Baldini, U. De Giovannini, H. Hübener, and A. Rubio, Phys. Rev. Lett. **129**, 167401 (2022).
[8] X. Li, T. Qiu, J. Zhang, E. Baldini, J. Lu, A. M. Rappe, and K. A. Nelson, Science **364**, 1079 (2019).
[9] T. F. Nova, A. S. Disa, M. Fechner, and A. Cavalleri, Science **364**, 1075 (2019).
[10] S. Pal, N. Strkalj, C.-J. Yang, M. C. Weber, M. Trassin, M. Woerner, and M. Fiebig, Phys. Rev. X **11**, 021023 (2021).
[11] G. A. Samara, J. Phys. Condens. Matter **15**, R367 (2003).
[12] H. Fujishita, S. Kitazawa, M. Saito, R. Ishisaka, H. Okamoto, and T. Yamaguchi, J. Phys. Soc. Jpn. **85**, 074703 (2016).
[13] C. H. Perry, R. Currat, H. Buhay, R. M. Migoni, W. G. Stirling, and J. D. Axe, Phys. Rev. B **39**, 8666 (1989).
[14] G. Shirane and Y. Yamada, Phys. Rev. **177**, 858 (1969).
[15] J. F. Scott, Rev. Mod. Phys. **46**, 83 (1974).

[16] I. A. Akimov, A. A. Sirenko, A. M. Clark, J.-H. Hao, and X. X. Xi, Phys. Rev. Lett. **84**, 4625 (2000).

[17] P. A. Fleury and J. M. Worlock, Phys. Rev. Lett. **18**, 665 (1967).

[18] P. A. Fleury and J. M. Worlock, Phys. Rev. **174**, 613 (1968).

[19] Y. Ichikawa, M. Nagai, and K. Tanaka, Phys. Rev. B **71**, 092106 (2005).

[20] R. Mankowsky, A. von Hoegen, M. Först, and A. Cavalleri, Phys. Rev. Lett. **118**, 197601 (2017).

[21] See Supplemental Material at http://link.aps.org/supplemental/10.1103/PhysRevLett.130.126902 for experimental technique, fit to the non-oscillatory component of the terahertz-induced second harmonic generation signal, simulation of the coherent soft-mode oscillation.

[22] H. Vogt, Phys. Rev. B **51**, 8046 (1995).

[23] S. Cabuk, Phys. Status Solidi (b) **247**, 93 (2010).

[24] I. Katayama, H. Aoki, J. Takeda, H. Shimosato, M. Ashida, R. Kinjo, I. Kawayama, M. Tonouchi, M. Nagai, and K. Tanaka, Phys. Rev. Lett. **108**, 097401 (2012).

[25] O. Aktas, S. Crossley, M. A. Carpenter, and E. K. H. Salje, Phys. Rev. B **90**, 165309 (2014).

[26] C. A. D. Horst, S. Magnien, and S. Kapphan, Ferroelectrics **185**, 265 (1996).

[27] I. N. Geifman and I. S. Golovina, Ferroelectrics **199**, 115 (1997).

[28] Z. Trybuła, S. Miga, S. Łoś, M. Trybuła, and J. Dec, Solid State Commun. **209–210**, 23 (2015).

[29] C. A. der Horst, J. Licher, S. E. Kapphan, V. Vikhnin, and S. Prosandeyev, Ferroelectrics **264**, 261 (2001).

[30] B. E. Vugmeister and M. D. Glinchuk, Rev. Mod. Phys. **62**, 993 (1990).